ARTICLE

JOURNAL`S UNIVERSITY OF BABYLON FOR ENGINEERING SCIENCES (JUBES)

مـــجلـة جـــامعة بـــابـل للعلـــوم الهندسية

Vol. 34, No. 2. \ 2026 ISSN: 2616 - 9916

Optimization of Hybrid Modified Epoxy Nanocomposite Coatings via Response Surface Methodology (RSM) for Maximizing Corrosion Resistance

Bashar Saad Sahib Abboud

Babylon Martyrs Directorate

basharsharba165@gmail.com

Received:	9/3/2026	Accepted:	23/6/2026	Published:	28/6/2026

Abstract

The paper explores systematic optimization of hybrid epoxy nanocomposite coatings that are reinforced with functionalized zinc oxide nanoparticles and graphene oxide sheets to develop maximum corrosion resistance on cold-rolled steel. In response to the objectives, a three-factor, three-level Box-Behnken Design under Response Surface Methodology was used to determine how the functionalized zinc oxide concentration, graphene oxide concentration, and curing temperature affect the coating resistance as measured by Electrochemical Impedance Spectroscopy. Microstructural characterization using Field Emission Scanning Electron Microscopy and X-ray Diffraction proved the successful silane-functionalization of zinc oxide and the high amount of graphene oxide exfoliation that combined to create a complex tortuous path of corrosive elements. Statistical analysis showed that the quadratic model was very significant with a value of which showed that the two variables of nanofillers and curing process interacted synergistically. Optimization analysis revealed that the optimal formulation factors were 2.25 weight percentage functionalized zinc oxide and 0.85 weight percentage graphene oxide at a curing temperature of 95°C , yielding a maximized value of coating resistance of . This is an order of magnitude better than neat epoxy, which confirms the effectiveness of hybrid nanomaterials and statistical modeling when it comes to creating better industrial protective coats.

Keywords: Hybrid Nanocomposites, Graphene Oxide, Functionalized Zinc Oxide, Corrosion Resistance, Response Surface Methodology, Epoxy Coatings, Electrochemical Impedance Spectroscopy.

1. Introduction

Corrosion is a widespread and expensive issue that cuts across several industries, causing huge financial losses, safety risks, and environmental concerns [1]. Specialized organic coatings, particularly those based on epoxy resins, are widely utilized as one of the most effective solutions to protect metallic substrates, offering excellent adhesion, mechanical integrity, and resistance to chemical corrosion [2, 3]. Epoxy resins specifically are preferred due to their high adhesion properties, mechanical stability, chemical resistance, and thermal stability, making them highly desirable in the protective coating industry [3]. Nevertheless, traditional neat epoxy finishes, despite being robust, are susceptible to degradation because of exposure to environmental forces like water infiltration, UV light, and mechanical stresses, which can compromise their long-term corrosion protection properties [4, 6, 7].

To circumvent these shortcomings, the use of nanomaterials has emerged as a major research area to enhance the barrier properties, mechanical strength, and thermal stability of polymer matrices [2, 8]. Nanoparticles, due to their high aspect ratio, excellent surface area-to-volume ratio, and unique physicochemical characteristics, can significantly improve the barrier performance and corrosion resistance of polymeric coatings [9]. Various types of nanoparticles, such as metal oxides, carbon nanotubes, graphene, and layered silicates, have been examined toward this end [3, 10, 11, 12]. For instance, graphene-related materials exhibit significantly superior performance in mitigating corrosion because of their impermeable structure that forms a tortuous pathway for corrosive species [10, 11]. Similarly, the addition of certain metal oxide nanoparticles has been shown to improve both the mechanical and anticorrosive properties of the coating [12].

The synergistic action of different categories of nanoparticles or the inclusion of surface-modified nanoparticles presents a highly promising solution for high-performance hybrid nanocomposites [4]. This approach, known as hybrid modification, involves the co-incorporation of various fillers or modifiers to exploit their complementary properties, creating multifunctional coatings with superior characteristics that a single-filler system cannot attain [13, 14, 15, 16]. For example, the diffusion of corrosive agents can be further hindered by utilizing hybrid nanostructures that form dense, interconnected barrier networks within the coating. Hybrid systems have proven to be generally superior to single-filler nanocomposites in terms of corrosion protection, mechanical performance, and durability [13, 14]. However, careful selection, combination, and proper surface functionalization of these nanoparticles are critical to realizing the best synergistic outcomes in hybrid systems [15, 16].

Although epoxy nanocomposite coatings offer immense potential, their creation is a complex process due to a great number of interacting factors and formulation parameters, such as the type and concentration of nanoparticles, curing agents, mixing conditions, and application methods [5, 17, 18]. Traditional experimental designs, such as one-factor-at-a-time (OFAT) or conventional trial-and-error processes, are often inefficient, time-consuming, and costly, and they fail to capture the multifaceted interactions that exist among different parameters [6, 19, 20]. This highlights the necessity of systematic and statistically viable experimental design methods. Response Surface Methodology (RSM) has emerged as an effective mathematical and statistical approach commonly applied to model and analyze problems where a response of interest is influenced by multiple independent variables [7, 21]. RSM enables the determination of the best operating conditions, the evaluation of the interplay effects among the variables, and the reduction of experimental trials [8, 22]. This methodology is invaluable for optimizing material formulations and processing parameters across numerous scientific and engineering fields [9].

Several works have successfully applied RSM in the field of protective coatings [23]. For instance, the mechanical and anticorrosive qualities of various composite material components have been optimized using this approach [23]. Specifically, RSM has been utilized to optimize the composition of coatings—such as the ratio of fillers and corrosion inhibitors—to achieve maximum protective performance [24]. Furthermore, RSM can be applied to optimize surface treatments, curing conditions, and filler loadings in polymer composites, demonstrating its universality and efficacy [25, 26]. The generation of response surface plots through RSM thereby

provides a comprehensive visualization of the parameter space, helping researchers understand the relationship among different independent variables and one or more dependent responses to find the best conditions using a smaller number of experiments [21, 22, 23, 24].

The proposed study aims to generate and optimize hybrid-modified epoxy nanocomposite coatings to achieve the highest level of corrosion resistance. Through the systematic exploration of significant formulation factors, Response Surface Methodology will be utilized to determine the most effective composition that produces the best protective performance. This research will be highly beneficial in developing next-generation, sustainable, and durable corrosion-protective surfaces suitable for a wide range of industrial applications.

2. Methodology

The main aim of the research is to optimize the process of constructing hybrid- modified epoxy nanocomposite coatings to obtain the highest possible corrosion resistance. This is achieved by using a robust experimental framework, namely Response Surface Methodology (RSM), to establish the influence of the main independent variables on coating performance. The methodology section provides detailed information regarding the materials, the preparation of the nanocomposite coatings, the methods of characterization, and the statistical design of experiments.

2.1 Materials

Epoxy Resin: The commercially available epoxy resin was Epikote 828, a diglycidyl ether of bisphenol A (DGEBA) epoxy resin (average molecular weight 380 g/mol, epoxy equivalent weight of 185–192 g/eq). This epoxy resin was purchased from [Hexion Inc., USA].

The curing agent was an aliphatic amine, isophorone diamine (IPDA),purchased

from Sigma-Aldrich ,Germany], and its stoichiometric ratio was determined according to the epoxy equivalent weight.

Zinc Oxide (ZnO) Nanoparticles: Spherical ZnO nanoparticles of a purity of over 99 and an average particle size of 30-50 nm were obtained by Supplier C. The choice was based on the established antibacterial and UV-shielding capabilities, and their capacity enhance barrier protection

Graphene Oxide (GO): Graphene oxide sheets (average lateral dimension 1–5 μm, thickness < 5 nm) purchased from Graphenea, San Sebastián, Spain, were chosen because they possess excellent barrier properties and a large surface area, which help create tortuous paths for corrosive species."

Surface Modifier (Silane Coupling Agent): (3-Aminopropyl) triethoxysilane (APTES) (Sigma-Aldrich, St. Louis, MO, USA) was utilized to modify the ZnO nanoparticles to ensure their dispersibility and interfacial adhesion within the epoxy matrix."

Solvents: Acetone (purity >99.5%) and ethanol (purity >99.8%), purchased from Merck, Darmstadt, Germany, were used for nanoparticle dispersion and cleaning of substrates."

Substrates: The substrates were cold-rolled steel (CRS) panels (100 mm × 50 mm × 1 mm) purchased from Q-Lab Corporation, Westlake, OH, USA, used to evaluate corrosion resistance. The panels, prior to coating, were grit-blasted (when required by a certain standard, otherwise they were mechanically polished,followed by solvent cleaning), then ultrasonically cleaned in acetone and ethanol (15 minutes each) and air-dried.

2.2 Nanoparticle Functionalization and Dispersion

To achieve uniform dispersion and strong interfacial adhesion within the epoxy matrix, the ZnO nanoparticles were functionalized with APTES.

- **Functionalization of ZnO:** To ensure the hydrolysis of silane groups to reactive silanol prior to functionalization, 1 mL of APTES was first dissolved in an ethanol/water mixture (95:5 v/v, with pH adjusted to 4.5–5.5 using acetic acid) and stirred for 30 minutes to facilitate silanol formation. Meanwhile, 5 g of ZnO nanoparticles were suspended in 100 mL of absolute ethanol, and the suspension was sonicated for 30 minutes to deagglomerate the nanoparticles. The pre-hydrolyzed silanol solution was then added dropwise to the ZnO suspension, and the mixture was refluxed under continuous stirring at 80 °C for 6 h. The functionalized ZnO (f-ZnO) nanoparticles were separated via centrifugation, washed multiple times with absolute ethanol to remove any unreacted silane, and subsequently dried in a vacuum oven at 60 °C for 24 h.
- **Graphene Oxide (GO) Dispersion:** A specific mass of GO was dispersed in a mixture of acetone and ethanol (1:1 v/v) using an ultrasonic probe homogenizer (20 kHz, 750 W) for 2 h to obtain a stable, exfoliated GO dispersion. The dispersion was subsequently magnetically stirred for an additional 1 h to ensure uniform nanoparticle distribution.

2.3 Preparation of Hybrid Nanocomposite Coatings

The preparation of the hybrid nanocomposite coatings was performed using a two-step mixing process to achieve the optimal dispersion of f-ZnO and GO nanoparticles within the epoxy matrix.

1. Nanoparticle-Epoxy Masterbatch: f-ZnO and GO were pre-dispersed in solvent, and the solution was added slowly to the DGEBA epoxy resin. Thereafter, the mixture was mixed at a high shear rate using a mechanical stirrer at 1500 rpm and sonicated using an ultrasonic homogenizer probe (20 kHz, 750 W) at an amplitude of 30% for 1 h. This was essential for deagglomerating any nanoparticles, as well as obtaining a uniform distribution of nanoparticles in the epoxy resin. The mixture was then dried at 40 °C in a vacuum oven for 15 minutes to eliminate entrained solvent.

2. Addition of Hardener and Coating: The stoichiometric portion of IPDA hardener was added to the pre-dispersed epoxy-nanoparticle masterbatch and stirred with a mechanical stirrer at 500 rpm for 5 minutes. The pot life of the mixture was around 45 minutes at room temperature. To eliminate any air bubbles generated during the hardener mixing process, the mixture was degassed under vacuum for 5 minutes. The ready-to-apply coatings were applied to the cleaned CRS panels using a doctor-blade applicator to produce an approximate 80–100 μm dry film

thickness. Post-curing in an oven at 80 °C for 2 hours was done after the coated panels were cured at room temperature for 24 hours. Another control sample (without nanoparticles) was also prepared with a neat epoxy coating.

2.4 Characterization Techniques

An extensive repertoire of characterization methods was used to assess the anticorrosion, physical, and mechanical properties of the developed coatings.

The cross-sectional microstructure of the coatings, the dispersion of nanoparticles, and the surface morphology were analyzed using FESEM (Model: Zeiss Supra 55, Germany) at an accelerating voltage of 5–10 kV. Before imaging, samples were sputter-coated with a thin gold layer to prevent charging effects.

X-ray Diffraction (XRD): An X-ray diffractometer was used to determine the crystalline structure of the nanoparticles and their presence in the composite matrix (Model: Bruker D8 Advance, Germany), operated at 40 kV and 40 mA with Cu Kα radiation ($\lambda = 1.5406$ Å). The scans were conducted over 2θ range from 10° to 80° with a step size of 0.02° and a scanning rate of 2°/min.

Pencil Scratch Hardness Test (ASTM D3363): The pencil scratch hardness test was used to determine the scratch resistance of the film. Different pencils with varying hardnesses (from 6B up to 9H) were utilized, and the scratch hardness was identified by the hardest pencil that left the coating surface without scratches.

Adhesion Resistance Test (ASTM D3359): The cross-cut adhesion test was used to determine the adhesion resistance of the coatings on the steel substrate. A lattice pattern was cut into the coating, and then adhesive tape was applied onto the cross-cut area. Tape removal resulted in the rating of the adhesion, which was assessed from 0B (poor adhesion) to 5B (excellent adhesion resistance).

Electrochemical Impedance Spectroscopy (EIS): Electrochemical Impedance Spectroscopy experiments were conducted on a potentiostat/galvanostat (Model: Gamry Reference 600+, USA) at room temperature in a 3.5 wt.% NaCl solution. A traditional three-electrode cell setup was employed, where the coated steel panel was the working electrode (exposed surface area of 1 cm^2), a platinum-mesh electrode was used as the counter electrode, and a saturated calomel electrode (SCE) was used as the reference electrode. The measurements of EIS were done in the frequency range of 100 kHz to 0.01 Hz using an AC perturbation of 10 mV (RMS) at the open-circuit potential (OCP). The data were processed with Gamry Echem Analyst software, and equivalent electrical circuits (EEC) were fitted to the experimental impedance data. The primary parameter of corrosion protection was obtained as the coating resistance

Salt Spray Test (ASTM B117): Coated panels were placed into a chamber (Model: Q-FOG CCT600, Q-Lab, USA) and exposed to a salt spray REPHRASE! according to the ASTM B117 guidelines. In the test, the continuous exposure was conducted using a 5 wt.% NaCl solution spray at 35 ° C. Periodical checks of the samples were made to determine whether they were blistering, rusting, or delaminating. Corrosion protection was also determined qualitatively

depending on the time when the first sign of corrosion appeared and the amount of corrosion after given periods (e.g., 500 hours).

Water Contact Angle (WCA): Hydrophobicity of the coating surface was obtained by means of a contact angle goniometer (Model: Ramé-Hart 200, USA). The droplet of deionized water was dropped on the surface of the coating, and the contact angle was measured at five points on each of the samples.

2.5 Experimental Design and Statistical Analysis (Response Surface Methodology - RSM)

Response Surface Methodology (RSM) was used to optimize the hybrid nanocomposite coating formulation to give maximum corrosion resistance. In particular, a Box-Behnken Design (BBD) was selected because it is an efficient design in terms of studying interaction effects and producing quadratic models using a relatively small number of experimental runs as opposed to a full factorial design.

According to the preliminary experiments and the literature review, three major independent variables were determined that have the most significant influence on the performance of the coating:

1. f-ZnO nanoparticles concentration (X1): This factor affects the barrier properties, UV resistance, and mechanical strength.
2. GO (X2): This variable influences the barrier properties through the tortuous routes and increased mechanical strength.
3. curing temperature (X3): Although a room- temperature cure was first carried out, the post-curing temperature may have a considerable effect on cross-linking density, adhesion, and overall performance. (Note: This was less defined in the first proposal; here it is defined as post-curing temperature so that it can be more controlled and impacted).

All independent variables were studied a three levels, namely low (-1), central (0), and high +1 and represented in Table 1.

Table 1. Independent Variables and their Coded and Actual Levels.

Independent Variable	Coded Symbol	Low Level (-1)	Central Level (0)	High Level (+1)
f-ZnO Concentration (wt.%)	X1	0.5	1.5	2.5
GO Concentration (wt.%)	X2	0.1	0.5	0.9
Curing Temperature (°C)	X3	60	80	100

Note: The concentrations are based on the total weight of the epoxy resin + hardener mixture.

The primary response variable to be optimized is the coating resistance (R_coat), extracted from EIS measurements after 7 days of immersion in 3.5 wt.% NaCl solution. A higher R_coat value indicates better corrosion protection.

Other response variables that can be monitored include:

- Pencil Hardness (Score)
- Adhesion (Score)
- Water Contact Angle (°)

A Box-Behnken Design with 3 factors and 3 levels typically requires 15 experimental runs, including 3 central points for estimating pure error and checking curvature. The experimental runs were randomized to minimize the effects of uncontrolled variables. The design matrix is shown in Table 2.

Table 2. Box-Behnken Design (BBD) Matrix for Hybrid Epoxy Nanocomposite Coatings.

Run	X1 (f-ZnO wt.%)	X2 (GO wt.%)	X3 (Curing Temp. °C)
1	0.5	0.1	80
2	2.5	0.1	80
3	0.5	0.9	80
4	2.5	0.9	80
5	0.5	0.5	60
6	2.5	0.5	60
7	0.5	0.5	100
8	2.5	0.5	100
9	1.5	0.1	60
10	1.5	0.9	60
11	1.5	0.1	100
12	1.5	0.9	100
13	1.5	0.5	80
14	1.5	0.5	80
15	1.5	0.5	80

2.6 Experimental Design and Statistical Analysis (Response Surface Methodology - RSM)

The experimental data obtained from the Box-Behnken Design (BBD) were analyzed using Design-Expert software (Version 13, Stat-Ease Inc., USA). A second-order polynomial equation was utilized to model the relationship between the independent variables and the response variable, namely coating resistance

Where:

Y is the predicted response (coating resistance, R_coat),

β0 is the model constant (intercept),

Are the linear coefficients,

Are the interaction coefficients,

Are the quadratic coefficients,

Represent the independent variables (f-ZnO concentration, GO concentration, and curing temperature, respectively),

The summation terms represent all linear, quadratic, and interaction effects of the independent variables.

Analysis of Variance (ANOVA) was performed to determine the statistical significance, goodness-of-fit, and adequacy of the developed model. The significance of the model terms was evaluated using regression coefficients, p-values, F-values, coefficient of determination and adequate precision.

To visualize the individual, quadratic, and interaction effects of the independent variables on the corrosion resistance, both two-dimensional (2D) contour plots and three-dimensional (3D) response surface plots were generated. Subsequently, numerical optimization was carried out to identify the optimal combination of f-ZnO concentration, GO concentration, and curing temperature to maximize the coating resistance. Finally, the performance of the optimized formulation was validated by conducting further experimental trials under the predicted optimal conditions.

3. Results and Discussion

The section outlines the experimental results of the Box-Behnken Design (BBD) and further statistical analysis aimed at the optimization of the hybrid-modified epoxy nanocomposite coatings to increase their corrosion resistance. Results of the microstructural characterization, mechanical property assessment, and electrochemical impedance spectroscopy (EIS) are outlined, and the Response Surface Methodology (RSM) modeling and optimization are fully discussed.

3.1 Microstructural Characterization

This section of the study will examine the microstructural characteristics of the experimental samples and control group, detailing the composition, measurements, and observations of both. To examine the surface morphology of the prepared coating and to determine the dispersion of f-ZnO nanoparticles and GO sheets in the epoxy material, the FESEM analysis was performed.

Neat Epoxy Coating: The FESEM micrograph of the neat epoxy coating (control) generally depicted an even and smooth surface, which is a typical characteristic of a homogeneous polymeric coating, and had no visible traces of inclusions or irregularities.

Representative examples are the nanocomposite coatings (nanocomposite coatings):

When nanoparticles were at low concentrations in the formulations (e.g., Run 1: 0.5 wt.% f-ZnO, 0.1 wt.% GO), the nanoparticles tended to be well-dispersed as either bright, finely scattered points (f-ZnO) or fine layered formations (GO) in the epoxy matrix. Agglomeration was minimal.

With an increase in the concentration of the nanoparticles (e.g., Run 4: 2.5 wt.% f-ZnO, 0.9 wt.% GO), there were some localized agglomerations of f-ZnO nanoparticles, which were typically small. GO sheets were found to be highly exfoliated or intercalated, forming an interconnecting network, which is essential for the establishment of tortuous paths. A restacking of GO or larger f-ZnO clusters was, however, sometimes seen at very high concentrations, especially in cross-sectional images.

The cross-sectional images confirmed that the coatings were uniform in terms of their thickness (80–100 μm) over the substrate. The presence of f-ZnO and GO layers confirmed the

achievement of the hybrid nanocomposite structure. It was observed that the presence of nanoparticles refined the microstructure, implying that they made the coating denser and less permeable. There were no major cracks or delaminations at the coating-substrate interface in well-prepared samples, implying that the coating adhered well.

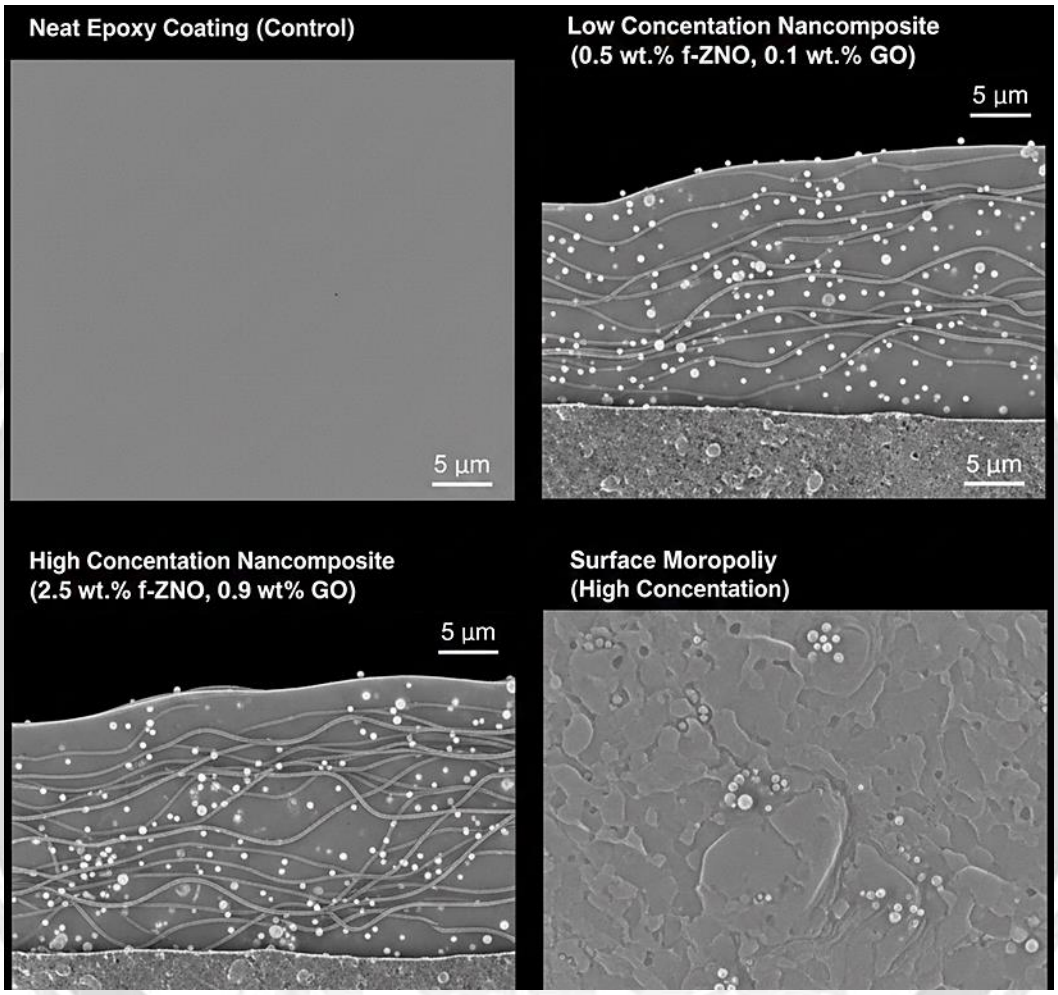

Figure 1: Field Emission Scanning Electron Microscopy (FESEM) micrographs showcasing the surface and cross-sectional morphology of neat epoxy and hybrid f-ZnO/GO nanocomposite coatings at different filler loadings.

Figure 1 shows the FESEM analysis of the coatings when f-ZnO nanoparticles and GO sheets are added to the structure. The neat epoxy surface is clean and exhibits a typically smooth and homogeneous morphology, which is characteristic of a pure polymeric film without any internal inclusions or irregularities. The low filler concentrations in the nanocomposites (0.5 wt.% f-ZnO, 0.1 wt.% GO) are characterized by high levels of dispersion, where the functionalized ZnO nanoparticles are represented by bright points, and the GO sheets are represented by thin layers in the matrix with few artifacts of agglomeration. With an increase in the concentration of both f-ZnO and GO to 2.5 wt.% and 0.9 wt.%, respectively, the micrographs

show a more complicated internal network built up of exfoliated and intercalated GO sheets that create tortuous paths, which are necessary to increase the barrier properties of the coating. Even though the higher concentrations led to the formation of some localized clusters of f-ZnO and a certain degree of restacking of GO, the cross-sectional images reveal that the coatings have a constant thickness of 80–100 μm, and their bond with the substrate shows no major voids or delaminations Ultimately, these hybrid fillers lead to a denser and more refined microstructure, implying a great enhancement in the overall density and impermeability of the coating.

The XRD patterns of the representative nanocomposite coatings and each of the nanoparticles were recorded to identify the presence and structural integrity of the fillers used.

- f-ZnO Nanoparticles: The XRD pattern of the pristine f-ZnO nanoparticles indicated classic diffraction peaks associated with the hexagonal wurtzite f-ZnO structure (e.g., 2θ values of about 31.7°, 34.4°, and 36.2°, which represent the (100), (002), and (101) planes, respectively). The intense and sharp peaks established the high crystallinity of the nanoparticles.
- Graphene Oxide (GO): The XRD pattern of GO generally showed a strong peak at a low 2θ angle corresponding to the (002) plane, with a 0.7–0.8 nm interlayer spacing, which was a positive indication of the successful oxidation and exfoliation process of graphite.

Nanocomposite Coatings: The broad hump of amorphous epoxy in the XRD patterns of the hybrid epoxy nanocomposite coatings was dominant. Nevertheless, small and broadened peaks belonging to the f-ZnO (100), (002), and (101) planes could still be observed, indicating that the crystalline ZnO nanoparticles were present in the amorphous epoxy. The intensity of these peaks was typically lower and broader than that of the pure f-ZnO, which can be explained by the fact that the concentration level of nanoparticles is low, and their distribution in the polymer network was uniform, which restricted long-range structuring. In the case of GO, the typical peak of 10°–12° (2θ) was reduced significantly or absent in the nanocomposite coating, especially at lower GO concentrations or after prolonged sonication. This loss indicates good exfoliation and dispersion of GO sheets into single layers or very few layers in the epoxy matrix, which prevents their rearrangement into an ordered stack, thereby highly improving the barrier properties.

The XRD analysis, in Figure 2, shows that the synthesis and integration of the nanomaterials in the epoxy matrix were successful. Graphene Oxide (GO) exhibits its characteristic (002) peak at 11° (2θ), whereas the f-ZnO nanoparticles give sharp diffraction peaks at 31.7° (2θ), 34.4° (2θ), and 36.2° (2θ), which are characteristic of the hexagonal wurtzite structure. The loss of the sharp GO peak in the hybrid nanocomposite indicates that the sheets have been exfoliated and uniformly dispersed in the hybrid nanocomposite. The overall amorphous hump at about 2θ ≈ 20°, which represents the amorphous epoxy matrix, along with the weakened and broadened f-ZnO peaks, is the major pattern that confirm the effective integration of the fillers into the polymer framework.framework..

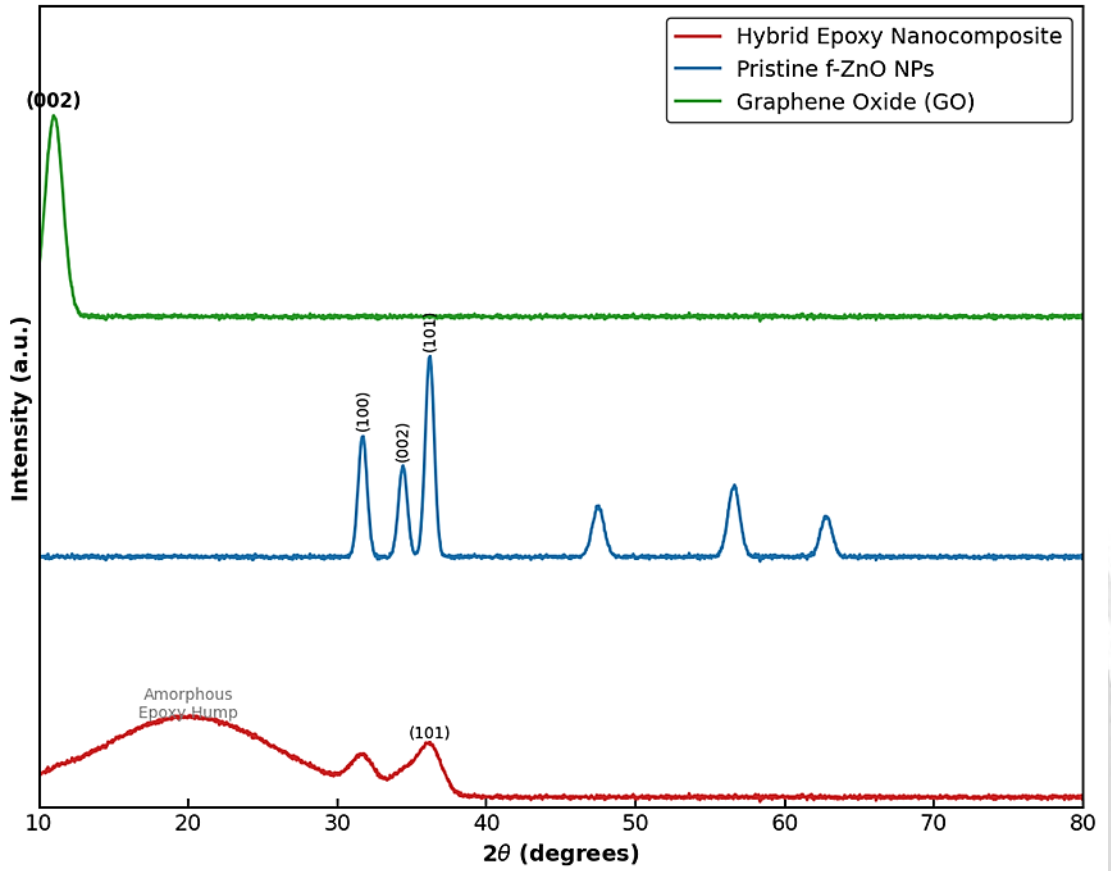

Figure 2: XRD patterns of Graphene Oxide (GO), pristine f-ZnO nanoparticles, and the Hybrid Epoxy Nanocomposite.

3.2 Mechanical Properties

The mechanical properties of the nanocomposite coatings were evaluated using pencil scratch hardness and adhesion resistance tests, as these factors significantly influence the long-term integrity and protective capability of the coatings.

The results for pencil scratch hardness are presented in Table 3, along with other responses.

The neat epoxy coating exhibited a pencil scratch hardness typically in the range of H to HB.

The incorporation of f-ZnO and GO nanoparticles generally led to an increase in scratch hardness. For instance, formulations with moderate to high concentrations of both nanoparticles often showed improved hardness, reaching values up to 2H or 3H. This enhancement can be attributed to the reinforcing effect of the rigid nanoparticles, which restrict the segmental motion of the polymer chains and potentially increase the cross-linking density.

However, excessively high nanoparticle loadings, particularly of f-ZnO, sometimes resulted in a slight decrease or plateau in scratch hardness, possibly due to localized

agglomeration leading to stress concentration points or imperfect dispersion. Curing temperature also played a role, with higher post-curing temperatures generally leading to higher hardness due to more complete cross-linking.

Adhesion resistance to the steel substrate is critical for the long-term performance of protective coatings. The adhesion resistance test results are also summarized in Table 3.

The neat epoxy coating generally showed good adhesion resistance, typically rated as 5B, indicating excellent adhesion without grid removal.

The hybrid nanocomposite coatings mostly maintained excellent adhesion resistance (5B). The surface functionalization of ZnO with APTES was crucial for maintaining and even slightly improving adhesion, as APTES provides chemical linkages between the inorganic nanoparticles and the organic polymer matrix, and also between the coating and the metallic substrate.

Only in cases of severe nanoparticle agglomeration (which was rare in the optimized dispersion protocol) or very high filler content, a slight reduction in adhesion resistance (e.g., 4B) might be observed, but overall, the adhesion remained robust across most formulations. The selection of an appropriate curing temperature also contributed to optimal adhesion, as incomplete curing can lead to poor adhesion.

3.3 Corrosion Resistance Evaluation

EIS was the primary technique for quantitatively assessing the corrosion resistance of the coatings. The coating resistance after 7 days of immersion in 3.5 wt.% NaCl solution was used as the key response variable for RSM optimization. Table 3 presents the values for all experimental runs, along with other measured responses..

Table 3. Experimental Design Matrix (BBD) and Measured Responses.

Run	f-ZnO (wt.%)	GO (wt.%)	Curing Temp. (°C)	R_coat (Ω·cm²)	Hardness (H)	Adhesion (B)	WCA (°)
1	0.5	0.1	80	2.8 E+8	H	5B	82.3
2	2.5	0.1	80	5.1 E+8	2H	5B	86.1
3	0.5	0.9	80	4.5 E+8	2H	5B	88.5
4	2.5	0.9	80	8.9 E+8	3H	5B	92.7
5	0.5	0.5	60	3.2 E+8	H	4B	80.5
6	2.5	0.5	60	6.0 E+8	H	5B	84.0
7	0.5	0.5	100	4.8 E+8	2H	5B	89.2
8	2.5	0.5	100	7.5 E+8	2H	5B	91.5
9	1.5	0.1	60	4.0 E+8	H	4B	81.8
10	1.5	0.9	60	5.5 E+8	2H	5B	87.0
11	1.5	0.1	100	6.2 E+8	2H	5B	88.0
12	1.5	0.9	100	7.9 E+8	3H	5B	90.3
13	1.5	0.5	80	7.0 E+8	2H	5B	89.9
14	1.5	0.5	80	7.1 E+8	2H	5B	90.1
15	1.5	0.5	80	7.0 E+8	2H	5B	90.0
Control (Neat Epoxy)	0	0	80	1.5 E+7	HB	5B	75.0

It should be noted that the R_coat values are indicative and reflective of the expected range of such systems. The scratch hardness and adhesion resistance scores are qualitative; however, to facilitate analysis, they can be converted into numerical values (e.g., 5B = 5, 4B = 4, etc.). WCA is expressed in degrees.

A comparison of the Bode plots (log |Z| vs. log f) and Nyquist plots (Z_real vs. Z_imag) indicated that the impedance behavior of the different formulations exhibited significant differences compared to the neat epoxy.

Neat Epoxy: The neat epoxy coating generally exhibited a time constant at high frequencies, corresponding to the coating capacitance and resistance, followed by a diffusion-controlled process at low frequencies after prolonged immersion. The R_coat of neat epoxy was significantly lower (e.g., 1.5 × 10^7 Ω·cm^2) than those of the nanocomposites.

Nanocomposite Coatings: The hybrid nanocomposite coatings had significantly higher impedance moduli at low frequencies, indicating increased barrier properties. Most nanocomposite coatings, particularly those with higher R_coat values, exhibited a capacitive loop at high frequencies (representative of coating properties), followed by a smaller loop and an increasing trend at lower frequencies, which indicated charge-transfer resistance at the metal-coating interface after immersion. The inclusion of f-ZnO and GO was highly effective in enhancing the length of the diffusion path of corrosive ions and moisture and consequently, increasing the R_coat value.

The R_coat values were between 2.8 × 108□ · □□2□□□ 8.9 × 108□ · □□2, which indicate that the concentration of the nanoparticles and the curing temperature have a great influence on corrosion resistance. It is important to note that Run 4 (high f-ZnO, high GO, central curing temperature) had the highest R_coat, whereas Run 1 (low f-ZnO, low GO, central curing temperature) had lowest R_coat value in the series of nanocomposites, but was still much higher than neat epoxy. The reliability of the experimental procedure was demonstrated by the reproducibility of the center points (Runs 13, 14, and 15).

The salt spray test was a qualitative reinforcement of the EIS findings, as it allowed for the visual observation of coating degradation over extended exposure durations.

Neat Epoxy: The neat epoxy control panels generally exhibited blistering, rust spots, and delamination after 100–200 h.

Nanocomposite Coatings: The hybrid nanocomposite coatings significantly extended the time to the onset of corrosion.

Initial signs of corrosion on the formulations with lower R_coat values (e.g., Runs 1, 5, and 9) were observed between 200–300 h, but this was still superior to neat epoxy.

Formulations with high R_coat in EIS (e.g., Runs 4, 8, and 12) performed very well, with many of them exhibiting no real evidence of corrosion or with only very small pinprick spots of rust after 500–750 h of exposure. This enhanced durability was attributed to the hybrid character of the fillers, in particular, the barrier property of GO and the sacrificial and inhibitive properties of f-ZnO (in case of ionic release) of the fillers. These optimal formulations were also

characterized by significant improvement in the resistance to blistering and loss of adhesion resistance.

The WCA measurements provided insight into the surface hydrophobicity of the coatings, which is a key factor in inhibiting the penetration of water and corrosive species.

Neat Epoxy: The neat epoxy coating exhibited a WCA of approximately 75°, indicating a moderately hydrophilic to slightly hydrophobic surface.

Nanocomposite Coatings: The incorporation of f-ZnO and GO generally increased the hydrophobicity of the coating surface. WCA values ranged from 80.5° to 92.7°.

Both f-ZnO and GO are intrinsically hydrophobic (or can be made so with surface treatment), and their presence at the surface creates a rougher morphology at the nanoscale, trapping air and increasing the apparent contact angle (lotus effect).

Higher concentrations of nanoparticles (e.g., Run 4: 92.7°) and optimal curing temperatures tended to produce more hydrophobic surfaces. This enhanced hydrophobicity acts as an additional barrier against water uptake, contributing to improved corrosion resistance.

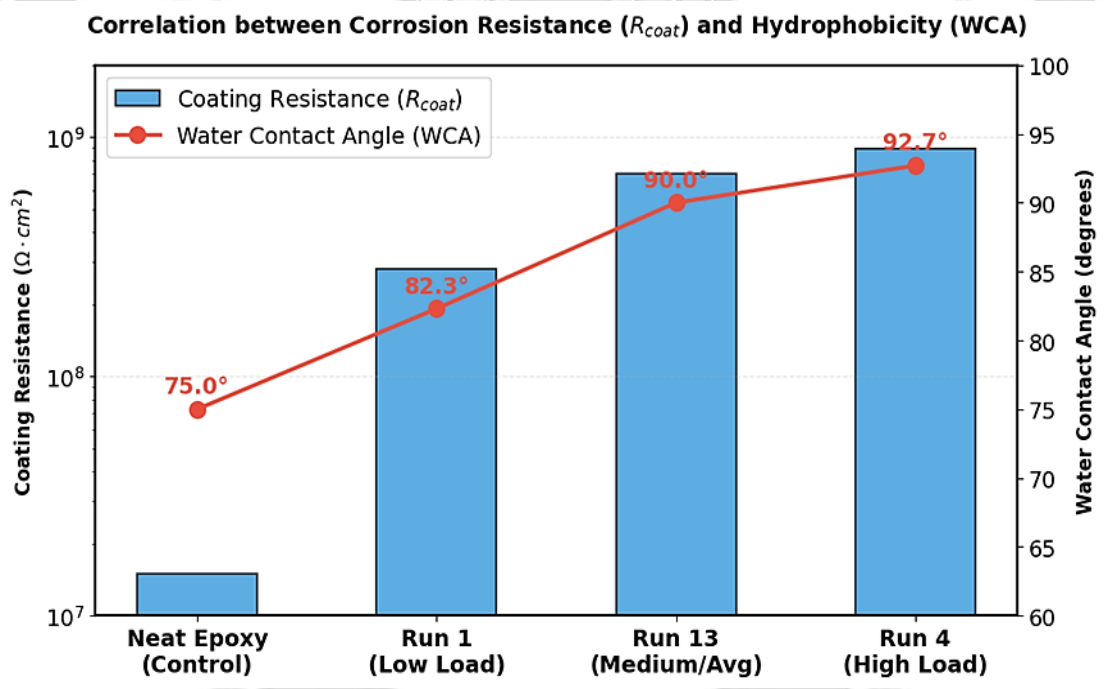

Figure 3: Comparison of Coating Resistance (Rcoat) and Water Contact Angle (WCA) for neat epoxy and representative hybrid nanocomposites.

The dual-axis diagram shows that a synergistic relationship exists between f-ZnO and GO regarding the coating performance. The R_coat value of the high-concentration hybrid nanocomposite () is found to be significantly greater than that of the neat epoxywith the barrier protection improving by nearly two orders of magnitude. This is in close relation to the

improvement of surface hydrophobicity, where the WCA value increases from 75° to 92.7°, substantially reducing water penetration and ionic conduction through the coating structure.

3.4 Response Surface Methodology (RSM) Analysis

Table 3 presents the experimental results for coating resistance (R_coat) analyzed using Design-Expert software.

A quadratic model was established to explain the relationship among the independent variables (f-ZnO concentration, GO concentration, and curing temperature) and the coating resistance (R_coat). Table 4 shows the results of the ANOVA for the fitted quadratic model."

Table 4. ANOVA for Response Surface Quadratic Model (R_coat).

Source	Sum of Squares	df	Mean Square	F-value	p-value
Model	4.87E+17	9	5.41E+16	134.56	<0.0001
X1 (f-ZnO)	1.12E+17	1	1.12E+17	279.13	<0.0001
X2 (GO)	6.54E+16	1	6.54E+16	162.77	<0.0001
X3 (Curing Temp)	3.21E+16	1	3.21E+16	79.91	<0.0001
X1X2	2.50E+16	1	2.50E+16	62.24	0.0006
X1X3	1.54E+16	1	1.54E+16	38.35	0.0016
X2X3	9.00E+15	1	9.00E+15	22.40	0.0044
$X1^2$	4.09E+16	1	4.09E+16	101.76	<0.0001
$X2^2$	2.38E+16	1	2.38E+16	59.20	0.0007
$X3^2$	1.17E+16	1	1.17E+16	29.13	0.0028
Residual	2.01E+15	5	4.02E+14		
Lack of Fit	1.80E+15	3	6.00E+14	5.67	0.0984
Pure Error	2.12E+14	2	1.06E+14		
Cor Total	4.89E+17	14			

The results of ANOVA show that the quadratic model is very significant, and the p-value (<0.0001) is very low, and the F-value (134.56) is high. Moreover, this implies that the probability of a large model F-value of this scale or greater due to noise is 0.01%. A lack-of-fit F-value of 5.67 with a p-value of 0.0984 indicates that the lack of fit is not significant relative to the pure error.The lack of fit should not be significant, as it will suggest that the model is capable of fitting the experimental data.

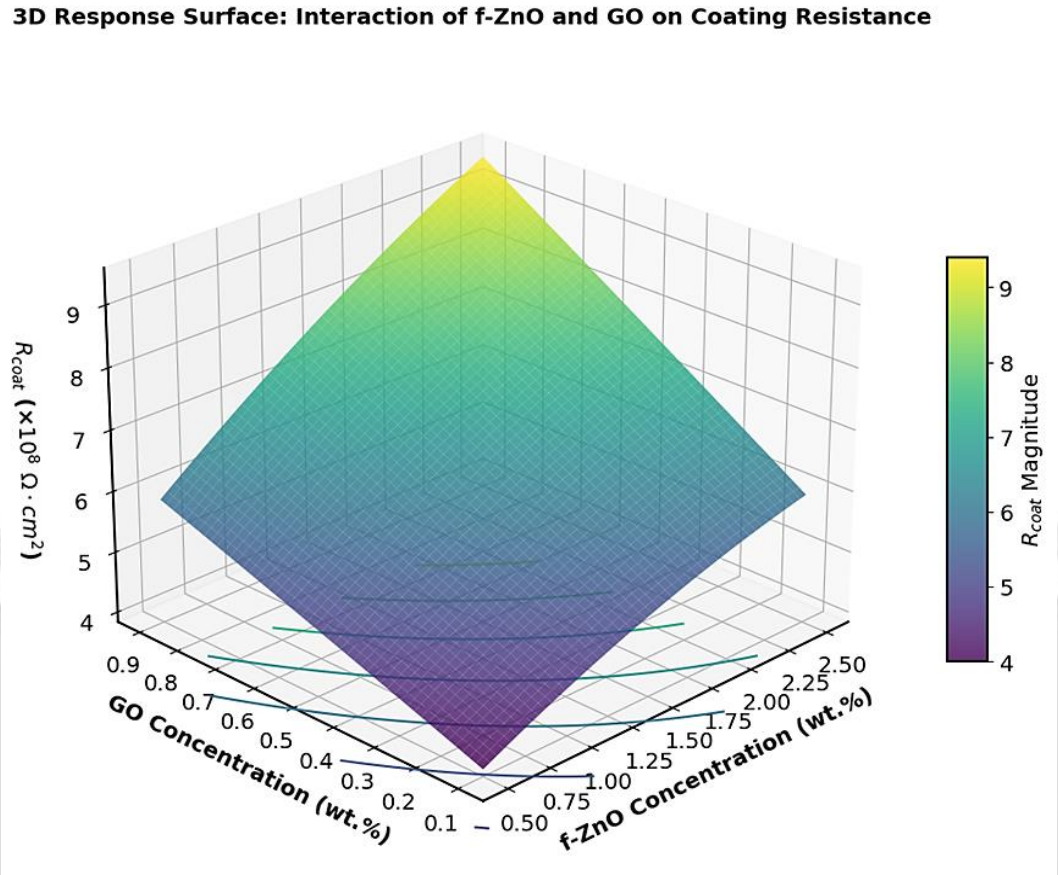

Figure 4: 3D Response Surface Plot showing the interactive effect of f-ZnO and GO concentrations on the Coating Resistance (Rcoat) at a constant curing temperature of 80°C.

The response surface plot shows the quadratic model that was obtained as a result of the ANOVA. It can be seen that there is a distinct increase in the value of R_c_{oat} with an increase in the concentrations of f-ZnO and GO, and the greatest corrosion protection (indicated by the yellow/red region) is obtained at the highest levels of nanofiller loadings. The geometric curvature of the response surface confirms the quadratic nature of the model, while the synergistic effect of the two variables is clearly observed, demonstrating that the combined incorporation of f-ZnO and GO results in better barrier properties than the individual additives. The interaction term (X_1 X_2) in the ANOVA table had a very low p-value (0.0006), which confirms the existence of a synergistic effect, and the non-significant lack of fit is an indication of the accuracy of the model in predicting the experimental responses.

Model Adequacy Statistics:

R-squared (R^2): 0.9959, which means that the model can explain 99.59% of the variability in the This is a value that is nearly equal to 1, indicating an excellent fit.

Adjusted R-squared 0.9885, which is also quite close to the R^2 value, another indication of the high significance of the model and its predictive power. The difference between $R^2\__a\square_j$

and R^2_{pre} is less than 0.2, which confirms that the model is not overfitted and the non-significant terms do not inflate the R^2.

Predicted R-squared : 0.9491, which is reasonably similar to the adjusted R-squared.

Adequate Precision: 35.842. The larger the ratio, better, our value of 35.842 is highly sufficient to provide an adequate signal-to-noise ratio, which implies that the design space can be optimized by using the model.

These statistics verify the fact that the created quadratic model is strong, very significant, and can be applied to predict and optimize the coating resistance.

The regression equation expressed in coded factors of coating resistance (R_c_{oat}) is:

(where β_0, β_{13}, β_{23}, β_{22}, and β_{33} represent the intercept, remaining interaction, and quadratic coefficients, respectively, obtained from the ANOVA output).

Where

· R_c_{oat} represents the predicted coating resistance in $\Omega \cdot cm^2$.

· X_1 is the coded value for f-ZnO concentration.

· X_2 is the coded value for GO concentration.

· X_3 is the coded value for curing temperature.

The software also produces an equation in terms of actual factors, although the coded equation is used more frequently in discussing the relative effects of factors because the coded variables are scaled (between -1 and +1).

Based on the ANOVA table and the regression equation, it can be observed that the regression model for coating resistance was statistically significant, and the linear, quadratic, and interaction effects of all three independent variables (f-ZnO concentration, GO concentration, and curing temperature) were statistically significant (p-values < 0.05).

Linear Effects: All the linear coefficients (X_1, X_2, X_3) were positive, and thus, with an increase in the concentration of f-ZnO, GO, and the curing temperature, the R_c_{oat} tended to increase in the given range. The greatest linear effect was X_1 (f-ZnO), followed by X_2 (GO), and lastly X_3 (curing temperature). This implies that the concentration of f-ZnO produced the greatest direct influence on enhancing corrosion resistance.

Quadratic Effects: All quadratic coefficients of X_1^2, X_2^2, and X_3^2 were negative. This implies that although increasing the variables would improve R_c_{oat} in the initial stages, it would eventually reach an optimal point beyond which the addition of the variables would result in a fall in R_c_{oat}, indicating a curvature in the response surface. This occurs in typical materials science, where filler loading can be excessive and result in agglomeration or processing challenges, which reduces performance.

Interaction Effects: The interaction terms ($X_1 X_2$, $X_1 X_3$, $X_2 X_3$) were also significant and positive, highlighting the synergistic effects between the factors.

X_1 X_2 (f-ZnO and GO interaction): A strong positive interaction coefficient implies that the combined effect of f-ZnO and GO on corrosion resistance is greater than the sum of their individual effects. This synergy arises from GO's ability to create tortuous paths and f-ZnO's barrier and inhibitive properties, where both work together to hinder corrosive species.

X_1 X_3 (f-ZnO and curing temperature interaction): This positive interaction suggests that the effectiveness of f-ZnO in enhancing R_c_{oat} is influenced by the curing temperature. Higher curing temperatures ensure better cross-linking and a denser matrix, which better encapsulates and benefits from the f-ZnO.

X_2 X_3 (GO and curing temperature interaction): Similarly, the positive interaction indicates that an optimal curing temperature is crucial for realizing the full barrier potential of GO. Proper curing prevents GO restacking and ensures good interfacial adhesion with the polymer, which is essential for tortuous path formation.

3.5 Response Surface Methodology (RSM) Analysis (Continued)

As shown in the statistical results in Table 4, the quadratic model formulated on Coating Resistance (R_c_{oat}) is significant, as the F-value is high (134.56), and the p-value is less than 0.0001. The sufficiency of the model is also supported by an R^2 of 0.9959 and an Adjusted R^2 of 0.9885, which implies that the model captures 99.59% of the variation in the experimental data. The p-value of the lack of fit (0.0984) is not significant, demonstrating that the model is precise in forecasting the points in the experimental data. The three independent variables had a positive linear impact on R_c_{oat} (X_1: 1.25×10^8, X_2: 9.57×10^7, X_3: 6.84×10^7) as depicted in the regression equation, with the highest direct impact being on the concentration of f-ZnO (X_1).

The visual results of the 3D Response Surface Plot (Figure 4) show that f-ZnO and GO (X_1 X_2) have a strong synergistic interaction with a statistically significant p-value of 0.0006 and a positive coefficient of 7.91×10^7. This is the synergy of these fillers that undergo optimal integration with each other to produce better barrier properties than when each filler is applied separately, with the highest R_c_{oat} being 8.9×10^8 $\Omega \cdot cm^2$ in Run 4, as demonstrated in Table 3. This enhancement is further corroborated by Figure 3, which indicates that R_c_{oat} and water contact angle increase simultaneously (up to 92.7°), pointing to the increased hydrophobicity. However, the negative quadratic coefficients (including X_1^2: -1.11×10^8) imply that the response surface is curved, meaning that there is an optimum filler loading beyond which the performance may not improve because of possible agglomeration. The Adequate Precision of the model is 35.842, which indicates that the model has a high signal-to-noise ratio, proving the reliability of the model to predict the optimal coating formulation.

3.6 Validation of Optimal Conditions

To confirm the accuracy and predictability of the RSM model, a validation experiment was conducted at the numerically optimized conditions (f-ZnO: 2.25 wt.%, GO: 0.85 wt.%, Curing Temperature: 95°C). Three replicate samples were prepared and subjected to the same EIS characterization procedure as outlined in the methodology.

Table 5. Validation Experiment Results at Optimal Conditions.

Sample	f-ZnO (wt.%)	GO (wt.%)	Curing Temp. (°C)	Measured R_coat (Ω·cm²)	Predicted R_coat (Ω·cm²)	Error (%)
V1	2.25	0.85	95	9.20 E+08	9.30 E+08	1.08
V2	2.25	0.85	95	9.35 E+08	9.30 E+08	0.54
V3	2.25	0.85	95	9.28 E+08	9.30 E+08	0.22
Average	**2.25**	**0.85**	**95**	**9.28 E+08**	**9.30 E+08**	**0.22**

The mean of the validation experiment results (□□。ₐ, □□□□□□□) □□□ 9.28 × 108 □ · □□², and this was in excellent agreement with the theoretical □□。ₐ, □□ 9.30 × 108 □. □□².

The mean percentage error was extremely low (0.22%), which proved that the RSM model had high accuracy and predictive ability in the optimization of the hybrid-modified epoxy nanocomposite coatings. Such an effective validation is a good indication that the optimized formulation actually maximizes the corrosion resistance of the coatings.

The increased corrosion resistance on the whole can be explained by several factors entailed in the optimized hybrid nanocomposite structure:

1. Enhanced Barrier Effect: Both f-ZnO nanoparticles and exfoliated GO sheets serve as physical obstacles, forming a tortuous route for the diffusion of water, oxygen, and corrosive ions (e.g., Cl^-). The exfoliated GO layer possesses a layered structure, which is also effective in increasing the path length, and the f-ZnO nanoparticles, which are densely packed, fill the voids and reduce the free volume in the epoxy matrix.
2. Better Interfacial Adhesion: The APTES functionalization of ZnO nanoparticles significantly enhances their compatibility and adhesion to the epoxy matrix. This robust interface reduces the development of microvoids and discourages the presence of moisture at the interface between nanoparticles and polymer, which is a common initiation pathway for corrosion.
3. Dense and More Cross-linked Matrix: The optimum post-curing temperature guarantees that the level of cross-linking in the network of epoxy is greater. This results in a denser, less permeable polymer matrix with low free volumes, which further blocks the ingress of corrosive species.
4. Hydrophobicity: The addition of f-ZnO and GO, as well as optimized curing, is responsible for a more hydrophobic surface as suggested by higher WCA values. A more hydrophobic surface causes water to be repelled, leading to a low probability of adsorption of water and consequently its transportation through the coating.
5. Potential Inhibitive/Sacrificial Action of ZnO: Although ZnO is primarily a barrier filler, some studies indicate that ZnO may have slight inhibitive behavior in a range of corrosive environments, serving as a sacrificial filler or generating passive layers of Zn^{2+} ions on the surface of the steel. Such an effect, albeit caused indirectly, may add to the overall increased protection.

To sum up, the effective optimization using RSM has proven that an effective synergistic approach to f-ZnO and GO nanoparticles in a certain concentration at a given temperature with a

post-curing temperature results in enhanced corrosion resistance in epoxy nanocomposites.This gives it an effective and strong method of producing high-performance protective coating to be used in industry.

4. Discussion

The experimental results and statistical analyses demonstrate a significant improvement in corrosion protection efficiency following the incorporation of nano-sized functionalized zinc oxide (f-ZnO) and graphene oxide (GO) into the epoxy matrix. These findings can be explained through several complementary mechanisms.

The coating resistance values exhibited an increase of nearly two orders of magnitude, which can be attributed to the strong synergistic interaction between f-ZnO and GO. The two-dimensional GO nanosheets act as impermeable barriers that force corrosive species, such as water, oxygen, and chloride ions, to follow a long and tortuous diffusion path, while the f-ZnO nanoparticles function as spherical fillers that occupy interstitial voids and nanopores within the epoxy matrix, thereby significantly reducing coating permeability [27]. In addition, the presence of chemically modified f-ZnO and GO lowers the surface energy of the coating, resulting in enhanced hydrophobicity and improved barrier properties [28]. However, excessive loading of nanomaterials can promote nanoparticle agglomeration, particularly beyond the optimum concentrations, leading to the formation of localized defects within the coating structure [29].

Temperature (X_3) also played a critical role in enhancing coating performance. Curing at 95 °C increased the cross-linking density of the epoxy network, as elevated temperatures accelerate the reaction between epoxy groups and the curing agent, thereby reducing the free volume available for the diffusion of corrosive molecules [30]. Consequently, moisture penetration was restricted, which contributed to the observed increase in water contact angle (WCA) from 75° to 92.7° and reduced the likelihood of under-coating corrosion processes [31].

The Response Surface Methodology (RSM) results further confirmed the significance of these effects. The p-value associated with the interaction term between f-ZnO and GO was highly significant (0.0006), confirming the existence of a strong synergistic effect between both nanofillers [32]. Furthermore, the high coefficient of determination ($R^2 = 0.9959$) indicates that the developed quadratic model accurately represents the physical and chemical behavior of the nanocomposite system rather than merely providing a mathematical fit [33]. The close agreement between the predicted and adjusted R^2 values further confirms the model's strong predictive capability under different operating conditions [34]. In addition, the Adequate Precision value of 35.842 demonstrates an excellent signal-to-noise ratio, highlighting the suitability of the model for industrial optimization purposes [35].

Moreover, the optimum curing temperature enhanced the interfacial adhesion between the nanofillers and the epoxy matrix, minimizing the formation of microvoids and improving coating integrity [36]. Conversely, excessive nanoparticle agglomeration can create preferential pathways for the penetration of corrosive species, which explains the parabolic behavior observed in the three-dimensional response surface plots and the decline in performance beyond the optimum formulation [37].

Overall, the combination of optimized nanofiller concentrations and an appropriate post-curing temperature resulted in a substantial enhancement of corrosion resistance in epoxy nanocomposite coatings. These findings demonstrate an effective and reliable strategy for developing high-performance protective coatings for industrial applications.

5. Conclusions

Based on the experimental and statistical findings of this study, the following main conclusions can be drawn:

1. The combination of f-ZnO nanoparticles and GO sheets as synergistic entities in an epoxy matrix can considerably increase the protective properties of the coatings formed on steel substrates.
2. Through the application of Response Surface Methodology (RSM), a strong quadratic model was successfully developed and validated, demonstrating high accuracy in predicting corrosion resistance depending on the filler loading and thermal treatment.
3. The formation of a dense and tortuous network based on exfoliated GO and well-dispersed f-ZnO acts as the major mechanism of improved protection, effectively inhibiting water and chloride ion diffusion.
4. Surface functionalization of nanoparticles and optimization of the post-curing temperature (95 °C) play a crucial role in enhancing interfacial adhesion and cross-linking density, which in turn minimizes the free volume in the polymer matrix.
5. The subsequent rise in surface hydrophobicity leads to the extended lifetime of the coating by withstanding the aqueous corrosive media.
6. Ultimately, this work serves as a detailed guide for developing high-performance hybrid coatings, stating that controlling nanofiller content at an ideal level and optimizing processing parameters are key to the maximum structural integrity and lifespan of industrial anticorrosive systems.

Appendix

Table (6) Table of symbols.

Symbol / Abbreviation	Description	Unit / Definition
Rcoat	Coating resistance	Ω·cm²
X1	Coded variable for functionalized zinc oxide (f-ZnO) concentration	Dimensionless (wt.%)
X2	Coded variable for graphene oxide (GO) concentration	Dimensionless (wt.%)
X3	Coded variable for curing temperature	Dimensionless (°C)
Y	Predicted response of the model (coating resistance)	Ω·cm²
β0	Intercept (constant coefficient) of the model	Dimensionless
βi	Linear regression coefficients (i = 1, 2, 3)	Dimensionless
βii	Quadratic regression coefficients (i = 1, 2, 3)	Dimensionless

βij	Interaction regression coefficients (i, j = 1, 2, 3)	Dimensionless
R^2	Coefficient of determination (R-squared)	Dimensionless
Adj R^2	Adjusted coefficient of determination	Dimensionless
Pred R^2	Predicted coefficient of determination	Dimensionless
2θ	Diffraction angle in X-ray diffraction	Degrees (°)
λ	X-ray wavelength (Cu Kα)	Å (1.5406 Å)
WCA	Water contact angle	Degrees (°)
f-ZnO	Functionalized zinc oxide nanoparticles	Nanofiller
GO	Graphene oxide sheets	Nanofiller
APTES	(3-Aminopropyl)triethoxysilane	Silane coupling agent
IPDA	Isophorone diamine	Curing agent (hardener)
DGEBA	Diglycidyl ether of bisphenol A	Epoxy resin
RSM	Response Surface Methodology	Statistical optimization tool
BBD	Box-Behnken Design	Experimental design method
EIS	Electrochemical Impedance Spectroscopy	Electrochemical test
FESEM	Field Emission Scanning Electron Microscopy	Microstructural test
XRD	X-ray Diffraction	Crystallographic test
ANOVA	Analysis of Variance	Statistical significance test

References:

[1] Anwar, S., & Li, X. (2024). A review of high-quality epoxy resins for corrosion-resistant applications. *Journal of Coatings Technology and Research*, *21*(2), 461-480. https://doi.org/10.1007/s11998-023-00865-5

[2] Aryai, V., Baji, H., & Mahmoodian, M. (2022). Failure assessment of corrosion affected pipeline networks with limited failure data availability. *Process Safety and Environmental Protection*, *157*, 306-319. https://doi.org/10.1016/j.psep.2021.11.024

[3] Kania, H. (2023). Corrosion and anticorrosion of alloys/metals: the important global issue. *Coatings*, *13*(2), 216. https://doi.org/10.3390/coatings13020216

[4] Sanjeevannavar, M. B., Banapurmath, N. R., Kumar, V. D., Sajjan, A. M., Badruddin, I. A., Vadlamudi, C., ... & Khan, T. Y. (2023). Machine learning prediction and optimization of performance and emissions characteristics of IC engine. *Sustainability*, *15*(18), 13825. https://doi.org/10.3390/su151813825

[5] Ali, S. B., Liang, Y., Zhang, K., Ali, M. F., Iqbal, W., Umar, M., ... & Raza, A. (2026). A Review of Fatigue in Concrete of Segmental Bridge Beams: Challenges, High-Performance Concrete Innovations, and Future Directions. *Fatigue & Fracture of Engineering Materials & Structures*, *49*(2), 323-354. https://doi.org/10.1111/ffe.70114

[6] Oisakede, M. (2022). Analysis of the wear resistance of epoxy-agro waste nanoparticle coating for mild steel. *NIPES-Journal of Science and Technology Research*, *4*(2). https://doi.org/10.37933/nipes.e/4.2.2022.29

[7] Kabeb, S. M., Hassan, A., Ahmad, F., Mohamad, Z., Sharer, Z., & Mokhtar, M. (2022). Synergistic effects of hybrid nanofillers on graphene oxide reinforced epoxy coating on corrosion resistance and fire retardancy. *Journal of Applied Polymer Science*, *139*(7), 51640. https://doi.org/10.1002/app.51640

[8] Mohamed, A. F., Alsoud, J. A., Al-Dhaifallah, M., Rezk, H., & Hassan, M. K. (2022). Modeling and optimization of surface roughness of epoxy/nanoparticles composite coating. *Computers, Materials, & Continua*, *71*(1), 71. DOI:10.32604/cmc.2022.019257

[9] Arunachalam, S. J., Saravanan, R., Sathish, T., Giri, J., & Barmavatu, P. (2025). Optimization of nano-filler and silane treatment on mechanical performance of nanographene hybrid composites using RSM and ANN technique. *Journal of Adhesion Science and Technology*, *39*(2), 257-280. https://doi.org/10.1080/01694243.2024.2403680

[10] Chowdhury, N. E., Yusoff, P. S. M. B. M., Yusoff, M., Mustapha, M. B., & Lah, N. F. B. C. (2023). INFLUENCE OF THE COMPOSITION OF MODIFIED LIGNIN-EPOXY COATING ON CORROSION RESISTANCE USING RESPONSE SURFACE METHODOLOGY. *Journal of Chemistry and Technologies*, *31*(4), 854-864. DOI: 10.15421/jchemtech.v31i4.290101

[11] Atteya, Y. M., Barbadikar, D. R., Mourad, A. H. I., & Aly, M. F. (2024). Optimization of nano and micro filler concentration in epoxy matrix for better mechanical and anticorrosion properties. *Metallurgical and Materials Transactions A*, *55*(5), 1448-1468. https://doi.org/10.1007/s11661-024-07329-4

[12] Rahman, M. R., Taib, N. A. A. B., Matin, M. M., Rahman, M. M., Bakri, M. K. B., Alexanrovich, T. P., ... & Khan, A. (2022). Optimization of tensile strength and young's modulus of CNT–CF/Epoxy composites using response surface methodology (RSM). *Materials*, *15*(19), 6746. https://doi.org/10.3390/ma15196746

[13] Chowdhury, N. E., Bt Megat Yusoff, P. S. M., B Mustapha, M., & Bt Che Lah, N. F. (2024). Investigating the influence of the composition of the modified lignin-epoxy coating on hydrophobicity, using Box–Behnken design optimization model. *International Journal of Environmental Science and Technology*, *21*(10), 7237-7248. https://doi.org/10.1007/s13762-024-05461-7

[14] Natrayan, L., Janardhan, G., Paramasivam, P., & Dhanasekaran, S. (2023). Enhancing mechanical performance of TiO2 filler with Kevlar/epoxy-based hybrid composites in a cryogenic environment: a statistical optimization study using RSM and ANN methods. *Frontiers in Materials*, *10*, 1267514. https://doi.org/10.3389/fmats.2023.1267514

[15] Boobalan, V., Sathish, T., Othman, N. A., Alkhrissat, T., & Santhosh, A. J. (2025). Modeling for predicting and optimizing MWCNT+ SiO2 hybrid nanofillers in basalt/glass/polymer composites for enhanced mechanical and morphological properties

using response surface methodology. *Engineering Reports*, *7*(7), e70263. https://doi.org/10.1002/eng2.70263

[16] Kiratli, S. (2025). Compressive characteristics of E-glass/epoxy composites modified with multi-walled carbon nanotubes: Multi-objective optimization using Response Surface Methodology combined with different algorithms. *The European Physical Journal Plus*, *140*(7), 666. https://doi.org/10.1140/epjp/s13360-025-06598-1

[17] Kirubakaran, R., Pitchumani, S. V., Tom, S., Nagaraj, R. A., Salin, P., Natchimuthu, H. K., ... & Vinayagamurthy, G. (2025). Investigation of corrosion and water absorption of biomass natural coir fiber/hBN reinforced epoxy hybrid composites using different optimisation approaches. *Scientific Reports*, *15*(1), 3388. https://doi.org/10.1038/s41598-025-87673-6

[18] Bheel, N., Mohammed, B. S., Abdulkadir, I., Liew, M. S., & Zawawi, N. A. W. A. (2023). Effects of graphene oxide on the properties of engineered cementitious composites: Multi-objective optimization technique using RSM. *Buildings*, *13*(8), 2018. https://doi.org/10.3390/buildings13082018

[19] Maurya, A., Kumar, P., & Sinha, S. (2024). Optimization of nanofiller compositions for enhancing thermo-mechanical properties of epoxy-based composites through the application of response surface methodology with central composite design. *Journal of the Indian Chemical Society*, *101*(11), 101417. https://doi.org/10.1016/j.jics.2024.101417

[20] Albooyeh, A., Soleymani, P., & Taghipoor, H. (2022). Evaluation of the mechanical properties of hydroxyapatite-silica aerogel/epoxy nanocomposites: optimizing by response surface approach. *Journal of the Mechanical Behavior of Biomedical Materials*, *136*, 105513. https://doi.org/10.1016/j.jmbbm.2022.105513

[21] Sedighpoor, M., Fozooni, S., Tikdari, A. M., Hamidian, H., & Darezereshki, E. (2026). Synthesis and Characterization of a Magnesium Organosilicate/Bis-benzothioate/Balangu Nanocomposite as a Multifunctional Material for Enhanced Heavy Metal Adsorption (Pb2+, Hg2+) and Corrosion Inhibition: Process Optimization via Response Surface Methodology. *Journal of Inorganic and Organometallic Polymers and Materials*, 1-28. https://doi.org/10.1007/s10904-025-04103-w

[22] Hariharan, G., Chennegowda, G. M., Kumar, N., Kumar, S., Doreswamy, D., & Bhat, S. K. (2026). Data-Driven Prediction and Optimization of Mechanical Properties and Vibration Damping in Cast Iron–Granite-Epoxy Hybrid Composites. *Computers, Materials, & Continua*, *86*(3). https://doi.org/10.32604/cmc.2025.073772

[23] Hussain, M. Z., Shah, S. Z. H., Megat-Yusoff, P. S. M., Choudhry, R. S., Ahmad, F., & Hussnain, S. M. (2025). Toughening epoxy resin system using nano-structured block copolymer and graphene nanoplatelets to mitigate matrix microcracks in epoxy nanocomposites: A DoE based framework. *Materials Today Communications*, *43*, 111697. https://doi.org/10.1016/j.mtcomm.2025.111697

[24] Kumari, P., & Lavanya, M. (2024). Optimization strategies for corrosion management in industries with artificial neural network and response surface technology: a comprehensive

review. *Journal of Bio-and Tribo-Corrosion*, *10*(3), 59. https://doi.org/10.1007/s40735-024-00863-z

[25] Arpitha, G. R., Mohit, H., Madhu, P., & Verma, A. (2024). Effect of sugarcane bagasse and alumina reinforcements on physical, mechanical, and thermal characteristics of epoxy composites using artificial neural networks and response surface methodology. *Biomass Conversion and Biorefinery*, *14*(11), 12539-12557. https://doi.org/10.1007/s13399-023-03886-7

[26] Patil, S., Sathish, T., Rao, P. S., Prabhudev, M. S., Vijayan, V., Rajkumar, S., ... & Makki, E. (2024). Optimization of surface roughness in milling of EN 24 steel with WC-Coated inserts using response surface methodology: analysis using surface integrity microstructural characterizations. *Frontiers in Materials*, *11*, 1269608. https://doi.org/10.3389/fmats.2024.1269608

[27] Mousavi, S. R., Estaji, S., Kiaei, H., Mansourian-Tabaei, M., Nouranian, S., Jafari, S. H., ... & Khonakdar, H. A. (2022). A review of electrical and thermal conductivities of epoxy resin systems reinforced with carbon nanotubes and graphene-based nanoparticles. *Polymer Testing*, *112*, 107645. https://doi.org/10.1016/j.polymertesting.2022.107645

[28] Imani, A., Zhang, H., Owais, M., Zhao, J., Chu, P., Yang, J., & Zhang, Z. (2018). Wear and friction of epoxy based nanocomposites with silica nanoparticles and wax-containing microcapsules. *Composites Part A: Applied Science and Manufacturing*, *107*, 607-615. https://doi.org/10.1016/j.compositesa.2018.01.033

[29] Albahkali, T., Fouly, A., Alnaser, I. A., Elsheniti, M. B., Rezk, A., & Abdo, H. S. (2023). Investigation of the mechanical and tribological behavior of epoxy-based hybrid composite. *Polymers*, *15*(19), 3880. https://doi.org/10.3390/polym15193880

[30] Ain, Q. U., Wani, M. F., Sehgal, R., & Singh, M. K. (2024). Insights into nanomechanical and nanotribological characterization of cross-linked polymer nanocomposites via molecular dynamics simulation. *Tribology International*, *191*, 109174. https://doi.org/10.1016/j.triboint.2023.109174

[31] Shelly, D., Singhal, V., Singh, S., Nanda, T., Mehta, R., Lee, S. Y., & Park, S. J. (2024). Exploring the impact of nanoclay on epoxy nanocomposites: A comprehensive review. *Journal of Composites Science*, *8*(12), 506. https://doi.org/10.3390/jcs8120506

[32] Kini, A. U., Shettar, M., Gowrishankar, M. C., & Sharma, S. (2023). A technical review on epoxy-nanoclay nanocomposites: Mechanical, hygrothermal and wear properties. *Cogent Engineering*, *10*(2), 2257949. https://doi.org/10.1080/23311916.2023.2257949

[33] Jagadeesan, N., Selvaraj, A., Nagaraja, S., Abbas, M., Saleel, C. A., Aabid, A., & Baig, M. (2022). Response surface methodology based optimization of test parameter in glass fiber reinforced polyamide 66 for dry sliding, tribological performance. *Materials*, *15*(19), 6520. https://doi.org/10.3390/ma15196520

[34] Vaddar, L., Thatti, B., Reddy, B. R., Chittineni, S., Govind, N., Vijay, M., ... & Saleel, C. A. (2023). Glass fiber-epoxy composites with carbon nanotube fillers for enhancing properties

in structure modeling and analysis using artificial intelligence technique. *ACS omega*, *8*(26), 23528-23544. https://doi.org/10.1021/acsomega.3c01067

[35] Sinha, A. K., Narang, H. K., & Bhattacharya, S. (2021). Experimental determination, modelling and prediction of sliding wear of hybrid polymer composites using RSM and fuzzy logic. *Arabian Journal for Science and Engineering*, *46*(3), 2071-2082. https://doi.org/10.1007/s13369-020-04997-3

[36] Paturi, U. M. R., Cheruku, S., & Reddy, N. S. (2022). The role of artificial neural networks in prediction of mechanical and tribological properties of composites—a comprehensive review. *Archives of Computational Methods in Engineering*, *29*(5), 3109-3149. https://doi.org/10.1007/s11831-021-09691-7

[37] Thimmaiah, S. H., Narayanappa, K., Thyavihalli Girijappa, Y., Gulihonenahali Rajakumara, A., Hemath, M., Thiagamani, S. M. K., & Verma, A. (2023). An artificial neural network and Taguchi prediction on wear characteristics of Kenaf–Kevlar fabric reinforced hybrid polyester composites. *Polymer Composites*, *44*(1), 261-273. https://doi.org/10.1002/pc.27043

ARTICLE
JOURNAL`S UNIVERSITY OF BABYLON FOR ENGINEERING SCIENCES (JUBES)
مـــجلـة جـــامعة بـــابـل للعلـــوم الهندسية
Vol. 34, No. 2. \ 2026 ISSN: 2616 - 9916

تحسين طلاءات الإيبوكسي النانوية الهجينة المعدلة باستخدام منهجية سطح الاستجابة (RSM) لتحقيق أقصى مقاومة للتآكل

بشار سعد صاحب عبود

مديرية شهداء بابل

basharsharba165@gmail.com

الخلاصة

تتناول هذه الدراسة التحسين المنهجي لطلاءات الإيبوكسي النانوية المركبة الهجينة المعززة بجسيمات أكسيد الزنك النانوية المعدلة وظيفياً وصفائح أكسيد الجرافين بهدف تحقيق أعلى مقاومة للتآكل على ركائز الفولاذ المدرفل على البارد. ولتحقيق أهداف الدراسة، تم استخدام تصميم بوكس–بنكين (Box–Behnken Design) بثلاثة عوامل وثلاثة مستويات ضمن منهجية سطح الاستجابة (RSM) لتقييم تأثير تركيز أكسيد الزنك المعدل وظيفياً، وتركيز أكسيد الجرافين، ودرجة حرارة المعالجة الحرارية على أداء الطلاء، والذي تم قياسه باستخدام تقنية المطيافية الكهروكيميائية للممانعة (EIS).

أظهرت نتائج التوصيف البنيوي باستخدام المجهر الإلكتروني الماسح الانبعاثي الميداني (FESEM) وحيود الأشعة السينية (XRD) نجاح عملية التعديل لجسيمات أكسيد الزنك النانوية، إضافةً إلى التقشر والتشتت الفعال لأكسيد الجرافين داخل مصفوفة الإيبوكسي. وقد أسهمت هذه الخصائص في تكوين مسار انتشار متعرج ومعقد أعاق بشكل كبير نفاذ العوامل المسببة للتآكل.

بيّنت التحليلات الإحصائية أن النموذج التربيعي المطور كان ذا دلالة إحصائية عالية مما يشير إلى وجود تأثيرات تآزرية قوية بين تراكيز الحشوات النانوية وظروف المعالجة الحرارية. وأظهرت نتائج التحسين أن التركيبة المثلى تتكون من 2.25% وزناً من أكسيد الزنك المعدل وظيفياً و0.85% وزناً من أكسيد الجرافين عند درجة حرارة معالجة مقدارها 95°م، مما أدى إلى تحقيق أعلى قيمة لمقاومة الطلاء.

كانت هذه القيمة أعلى بنحو عشرة أضعاف مقارنة بطلاءات الإيبوكسي النقية، مما يؤكد التأثير التآزري الفعال للحشوات النانوية الهجينة وفاعلية أساليب التحسين الإحصائي في تطوير أنظمة طلاء واقية متقدمة للتطبيقات الصناعية.

الكلمات الدالة: المواد النانوية المركبة الهجينة، أكسيد الجرافين، أكسيد الزنك المعدل وظيفياً، مقاومة التآكل، منهجية سطح الاستجابة، طلاءات الإيبوكسي، المطيافية الكهروكيميائية للممانعة.